RSC Advances

PAPER

CrossMark
click for updates

Stable plasmonic Ag/AgCl–polyaniline photoactive composite for degradation of organic contaminants under solar light

Hossam A. Ghaly,[a] Amer S. El-Kalliny,[b] Tarek A. Gad-Allah,[b] Nour E. A. Abd El-Sattar*[c] and Eglal R. Souaya[c]

A series of novel plasmonic photocatalysts of Ag/AgCl–polyaniline (Ag/AgCl–PANI) were successfully synthesized by deposition–precipitation reaction followed by a photo-reduction method. The prepared photocatalysts were characterized by X-ray diffraction, field emission scanning electron microscopy, ultraviolet-visible diffuse reflectance spectroscopy, photoluminescence emission spectroscopy, and thermogravimetric analysis. Ag/AgCl–PANI was used to degrade methylene blue (MB) under simulated solar light. The effects of different parameters such as PANI content, initial pH and concentration of the MB solution, and catalyst dosage on the photo-degradation efficiency were assessed. Ag/AgCl–PANI plasmonic photocatalyst displayed much higher photocatalytic efficiency than the pure PANI or Ag/AgCl. The improved photocatalytic performances of the prepared photocatalysts were attributed to the high absorbance in the visible-light region, high surface areas of catalysts and the effective synergism of hetero-junction structure formed at the interface between Ag/AgCl and PANI, leading to improved separation of the photo-generated electron–hole pairs. A possible mechanism for the photo-degradation of MB molecules under simulated solar irradiation was suggested based on trapping experiments.

1. Introduction

Heterogeneous photocatalysis is an advanced oxidation process that can be applied in water and wastewater treatments for the degradation of organic pollutants through the formation of highly oxidizing hydroxyl radicals (HO•).[1] Most common photocatalysts are usually metal oxide semiconductors of wide band gap (*e.g.* TiO_2 and ZnO). The practical application of such photocatalysts is somewhat limited because they can be activated only by high energy UV irradiation (which only accounts for ~5% of solar spectrum) and possess rapid recombination of photo-generated charges.[2] Therefore, design and fabrication of new highly active visible-light-responsive photo-catalysts of small band-gap is an important issue to improve the utilization of the solar spectrum. In this context, two strategies should be considered: (1) improvement of the separation rate of photo-generated electron–hole pairs, and (2) expansion of the absorption edge to visible light.[3]

[a]*Reference Laboratory of Drinking Water, Holding Company for Water and Wastewater, Shubra El Kheima, Qalyubia, P.O. 13864, Egypt*

[b]*Water Pollution Research Department, National Research Centre, 33 EL Bohouth St. (former EL Tahrir St.), P. O. 12622, Dokki, Giza, Egypt*

[c]*Chemistry Department, Faculty of Science, Ain Shams University, Abbassia, 11566 Cairo, Egypt. E-mail: nour_ahmed1977@yahoo.com; nourel-dinahmed@sci.asu. edu.eg; Fax: +20224821031; Tel: +201012277219*

Recently, Zhou, *et al.* (2012) has utilized the phenomenon of surface plasmonic resonance (SPR) of noble metal nanoparticles (NPs) to develop a new type of photocatalysts which exhibit high photoactivity for decomposition of organic pollutants under UV-visible light irradiation.[4] This phenomenon comes from the collective oscillation of free conduction electrons on the surface of a noble metal, and can facilitate the separation of electrons and holes generated on the surface of the semiconductor.[4] Typical plasmonic photocatalysts include Ag/TiO_2, Au/TiO_2, Au/ZrO_2, Ag/Al_2O_3 and Ag/AgX.[4]

Among various plasmonic photocatalysts, silver/silver halide (Ag/AgX, X = Br, Cl, or I) displays excellent photocatalytic performance in the photo-degradation of organic pollutants under visible light irradiation because of the surface plasmonic resonance of Ag particles. Furthermore, production of oxidizing species such as Cl^0 or Br^0 from Ag/AgCl and Ag/AgBr, respectively, is possible.[5,6] However, the AgX species, prepared by traditional methods, suffer from some limitations concerning with their chemical stability that hinders their use in practical application. By the action of light, the photo-generated electrons combine with Ag ions (Ag^+) to form individual silver atoms (Ag^0), and finally a cluster of silver atoms is formed within the silver halide particle. This leads to instability for the photocatalytic activity of silver halides under irradiation.[5] Moreover, the low surface area of pure Ag/AgX, due to its tendency to agglomerate into larger particles, decreases its photoactivity.[7]

Also, plasmon-induced electron–hole pairs in Ag/AgX recombine before they arrive at the photocatalyst surface, leading to high rate of charge carriers recombination and decreases the plasmonic photoactivity.[8] Thus in principal, photoactivity and stability of Ag/AgX photocatalyst need to be further improved. Ag@AgCl/g-C$_3$N$_4$ plasmonic photocatalyst showed excellent photocatalytic performance under visible light irradiation for rhodamine B degradation with a rate constant higher than individual Ag@AgCl and g-C$_3$N$_4$.[9] Zhu et al.[6,10–12] utilized graphene oxide (GO) as a capping agent to fabricate Ag/AgCl/GO and Ag/AgBr/GO. The synergistic effect between the Ag/AgX and graphene oxide enhanced the photoactivity of the composite as it suppressed the recombination of electron–hole pairs in Ag/AgX/GO composite. Xu et al.[7] prepared SiO$_2$@Ag/AgCl plasmonic photocatalyst. The authors attributed the improved photocatalytic performance to the possibility of efficient diffusion and transportation of adsorbed organic molecules, to the increased number of interface active sites due to its high surface areas, and SPR effects of Ag NPs. These factors improve the efficiency of charge separation and make the catalysts more stable.

Polyaniline (PANI) can be considered as good substrate for photocatalysts due to its exceptional characters. For instance, it is the most famous easily prepared conducting polymer with an extended π-conjugated electron system,[13] behaves as narrow band gap (2.8 eV) semiconductor with high absorption coefficients in the visible light range, and acts as an excellent electron donor and a good hole acceptor when illuminated.[14,15] These unique properties make PANI used as photosensitizer for various semiconductors (e.g. Ag$_3$PO$_4$, g-C$_3$N$_4$, BiOCl, and TiO$_2$) in order to enhance the separation efficiency of photogenerated electron–hole pairs and consequently better photocatalytic activity and stability of photocatalyst could be achieved.[14–17] Ag@AgCl modified by PANI has been successfully prepared by other researchers and was used in different applications such as electronic, optics, electrocatalysis, and sensors.[18] However, this composite was not investigated as photocatalyst for water treatment, which might be a meaningful work to carry out. Thereby, Ag/AgCl–PANI composite was prepared with various amounts of PANI by deposition–precipitation reaction followed by photo-reduction method in this work. The obtained nanocomposite displayed high photocatalytic activity and good stability towards the photodegradation of Methylene Blue (MB) as a model compound for water contamination under simulated solar light.

2. Experimental

2.1. Materials

Silver nitrate (AgNO$_3$, 99%), hydrochloric acid (HCl, 36.5–38%), aniline (≥99.5%), ethyl alcohol, ammonium persulfate, benzoquinone and methylene blue were purchased from Sigma-Aldrich. Ammonium oxalate (AO) and isopropanol (IPA) were obtained from Fisher Chemicals Co. Deionized water (Milli-Q, Millipore, France) was used as the solvent in the preparation of all solutions and dispersions.

2.2. Synthesis of Ag/AgCl–PANI composite

PANI was prepared according to the method described by Wang et al.[15] Briefly, 0.5 mL of 0.09 M aniline was dissolved in 50 mL of 1 M HCl to produce a mixture solution (A). After that, 0.58 g of ammonium persulfate was dissolved in 50 mL of 1 M HCl as solution (B). Solution (A) was mechanically stirred for 1 h in an ice/water bath. Then, solution (B) was injected drop wisely to the cooled solution (A) using a syringe (2500 μL, Hamilton, Gastight, USA). The resultant mixture was allowed to react in the ice/water bath for 8 h. The final product was filtered and washed with deionized water and then ethanol. Finally, the powder was dried at 60 °C for 12 h in a drying oven (Heraeus, Germany).

The preparation of the Ag/AgCl–PANI composite was based on the method used by Bu and Chen.[14] First, 50 mg of the prepared PANI was dispersed into 25 mL of deionized water and the resulting mixture was ultrasonically vibrated (Branson 3510, USA) for 30 min. A pre-calculated amount of AgNO$_3$ was added into this mixture and the mixture was stirred for 6 h. Then, HCl solution (0.1 M) was slowly added drop by drop into the mixture of PANI and AgNO$_3$ solution under stirring. The stirring was continued for 24 h to form homogeneous suspension. After that, the suspension was centrifuged at 3000 rpm (Hermle Z 3000, Germany) to separate the AgCl–PANI powder and repeatedly washed with anhydrous ethanol and deionized water. Finally, the powder was dried at 80 °C for 24 h in a drying oven. Following the described procedure, different AgCl to PANI ratios could be prepared. Finally, the AgCl–PANI composite was mixed with distilled water and was irradiated by a 400 W metal halide lamp (Osram, Slovakia) for 10 min to reduce partly the adsorbed Ag$^+$ to Ag^0. Then, the precipitate was collected and dried in air. The Ag/AgCl–PANI composites with 2.5–20 wt% of PANI, (expressed hereafter as Ag/AgCl–PANI(x%), where x is the PANI wt%), were obtained after drying at 80 °C for 24 h. For the sake of comparison, a mechanical mixture of Ag/AgCl and 5% of PANI (denoted as Mm Ag/AgCl–PANI(5%)) was obtained by grinding 5 mg of PANI with 95 mg of Ag/AgCl. Pure Ag/AgCl, without the addition of PANI, was also prepared using the above mentioned method.

2.3. Characterization

The crystal structures of the samples were identified by X-ray diffraction (XRD) analysis using Bruker D8 diffractometer with Cu-Kα radiation (λ = 1.54 Å) in the 2θ range of 10–80°. The investigation of particles morphology and composition was performed using field emission scanning electron microscopy (FE-SEM, Quanta FEG 250, Japan). Thermal analysis was carried out for the dried Ag/AgCl–PANI(10%) using SDT Q600 V20.9 Build 20 equipment (TA Company, USA). The sample holder was heated in air at a rate of 10 °C min^{-1}, in the temperature range from ambient temperature up to 1000 °C. The specific surface areas of prepared samples were calculated from the N$_2$ adsorption/desorption isotherm at liquid-nitrogen temperature (77 K) using the Brunauer–Emmett–Teller (BET) equation. The isotherms were collected by Quantachrome NOVA automated gas sorption system. Optical properties were determined from the UV-visible diffuse reflectance spectra (DRS) obtained from

a spectrophotometer (Jasco-V-570, Japan). $BaSO_4$ was used as a reference material in the DRS measurements. Photoluminescence (PL) emission spectra of the samples were recorded at room temperature using RF-5301PC spectrophotometer (Shimadzu, Japan) with 320 nm excitation wavelength.

Point of zero charge (pH_{pzc}) refers to pH at which the electrical charge density on catalyst surface is equal to zero. pH_{pzc} was measured by the pH drift method.[19] In this method, pH of different 0.01 M NaCl solutions (50 mL) were adjusted to values between 2 and 12 using 0.1 M solution of either HCl or NaOH. About 0.05 g of Ag/AgCl–PANI(5%) was added into each solution at room temperature and then stirred for 30 min and final pH (pH_f) of solution was measured after 48 h. The difference between the initial pH (pH_i) and final one (pH_f–pH_i) was plotted against pH_i and the point where pH_f–pH_i = 0 was taken as the pH_{pzc}.[19]

2.4. Evaluation of the photocatalytic activity and active species trapping experiments

The application of Ag/AgCl–PANI composites for the degradation of MB dye was investigated under simulated sunlight irradiation using a 400 W metal halide lamp (the intensity was 40 000 lux measured by a light meter PCE 174, UK) located at a distance of 25 cm away from the upper surface of solution. The temperature of the reaction was controlled to 25 °C ± 2 by external cooling fan and monitored using data logger every 5 minutes. In a typical procedure, 70 mg of the photocatalyst powder was suspended in 70 mL of 10 mg L^{-1} MB solution. The suspension was stirred for 90 min in dark before irradiation to allow reaching the adsorption–desorption equilibrium of the dye on the photocatalyst surface. Afterward, the suspension was irradiated to initiate the photocatalytic process. Every 5 min, 3 mL sample was taken from the reaction system using a syringe and then centrifuged at 3000 rpm for 5 minutes to separate the photocatalyst particles. The degradation efficiency was monitored by recording the absorbance of MB dye at its maximum absorption wavelength (λ_{max} = 664 nm) using UV-visible spectrophotometer (Shimadzu 2550, Japan). Stability and reusability of the photocatalyst were carried out following the same procedure. After each photocatalytic cycle, the photocatalyst was collected by filtration and washed with deionized water, and finally dried at 80 °C in an oven before reuse.

In order to investigate the role of the reactive species generated in the photocatalytic reaction, IPA, AO, and BQ were added into the MB solution to trap $HO^{\bullet}$ radicals, holes (h^+) and superoxide radicals ($O_2^{\bullet-}$) species, respectively. Then, photocatalytic experiments were performed as mentioned previously.

3. Results and discussion

3.1. Characterization of Ag/AgCl–PANI composite

Crystallographic structure of the pure Ag/AgCl and the Ag/AgCl–PANI composites were identified from the XRD patterns illustrated in Fig. 1. No diffraction peaks characteristic for PANI were observed suggesting the low crystallinity of the PANI. The five characteristic diffraction peaks of AgCl (JCPDS file: 31-1238)
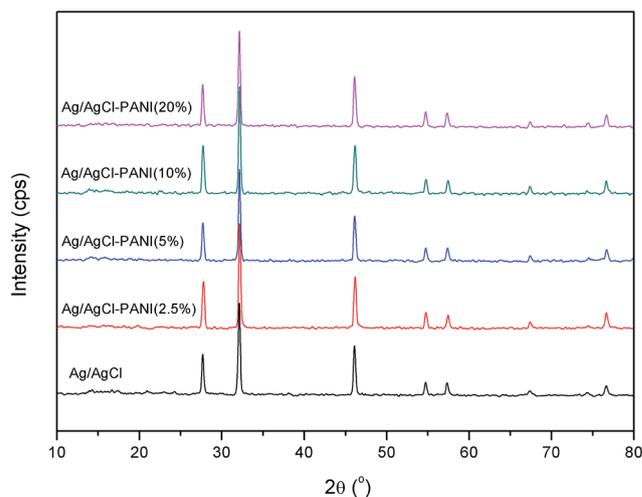

Fig. 1 XRD patterns of the prepared materials.

at $2\theta = 27.82°$, $32.24°$, $46.25°$, $54.81°$, and $57.56°$, corresponding to (111), (200), (220), (311), and (222) crystal planes, respectively, appear clearly in all samples. This means that addition of PANI does not change the lattice structure of AgCl in the Ag/AgCl–PANI composites and AgCl crystallized as a distinguishable phase in the composite. The characteristic diffraction peaks of Ag^0 were not observed in any sample. This is probably due to the low content of the metallic Ag produced photocatalytically on the surface of the AgCl particles. Another plausible explanation is the high dispersion of Ag^0 crystals on the surface of AgCl which was previously observed in Ag/AgCl/g-C_3N_4 porous nanosheets prepared by Zhang et al.[20] However, the presence of Ag^0 was confirmed by measuring the UV-visible diffuse reflectance spectra (DRS) as shown below.

The morphologies of PANI, Ag/AgCl and their composites with different ratios were observed under FE-SEM (Fig. 2a–d). Polyaniline was tubular in shape and tends to form an entangled network with an average diameter of 100 nm and a length of 500 nm similar to previous studies.[21] Pure Ag/AgCl consists of 0.8–1.5 μm irregularly shaped particles with relatively smooth surface as reported previously.[10,12] As can be seen in Fig. 2c, there are many PANI particles dispersed on the surface of Ag/AgCl particles. By increasing the content of PANI to 20%, not only a large number of PANIs cover the surface of Ag/AgCl, but also PANI can aggregate together (as shown in Fig. 2d). The aggregation of PANI could cause some limitations in the prepared photocatalyst, as it affected negatively on the surface area of the catalyst as shown latter in BET measurements, and shield the incident light reaching to Ag/AgCl particle. Moreover, aggregation of PANI affected negatively on the separation ability of the photo-generated electron and holes as seen latter in PL spectrum.

Pure Ag/AgCl and Ag/AgCl–PANI(5%) composite was analyzed by energy dispersive X-ray spectroscopy (EDS) technique (Fig. 2e and f). Cl and Ag peaks are observed in pure Ag/AgCl. In Ag/AgCl–PANI(5%), C peak appeared beside the peaks of Ag and Cl, which indicates the presence of PANI. N peak was not observed due to the low content of N in the composite. The
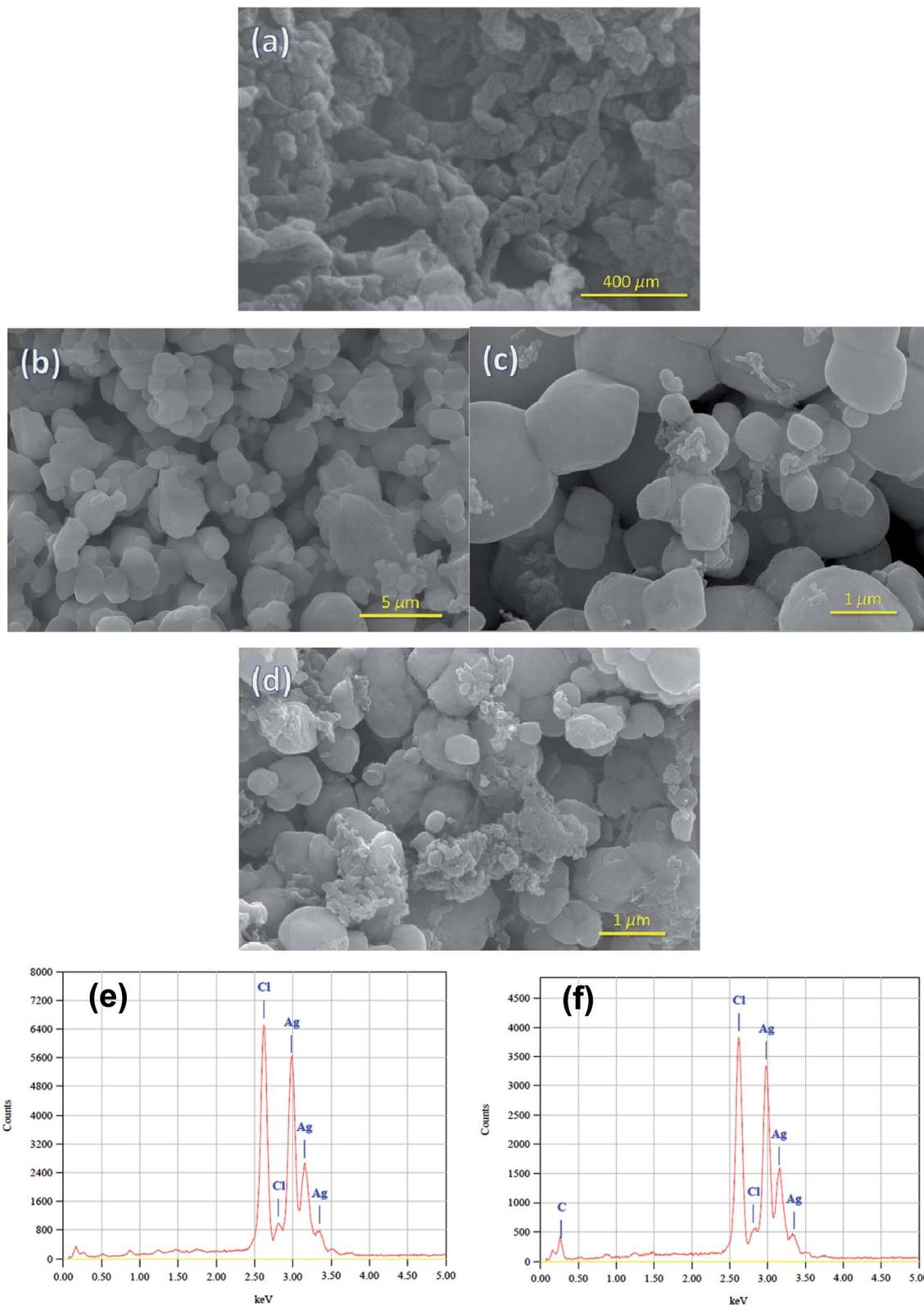
Fig. 2   FE-SEM images of (a) PANI, (b) Ag/AgCl, (c) Ag/AgCl–PANI(5%), and (d) Ag/AgCl–PANI(20%). (e and f) EDS of Ag/AgCl, Ag/AgCl–PANI, respectively.

EDS analysis indicates that Ag/AgCl and Ag/AgCl–PANI(5%) composite have no impurities.

To evaluate the thermal behavior and to determine the range of heat treatment of the prepared photocatalyst, Ag/AgCl–

PANI(10%) photocatalyst was subjected to thermo-gravimetric (TG) analysis and its differential form (DTG) as presented in Fig. 3. The first weight loss just below 100 °C can be ascribed to the evaporation of free water molecules and other volatile
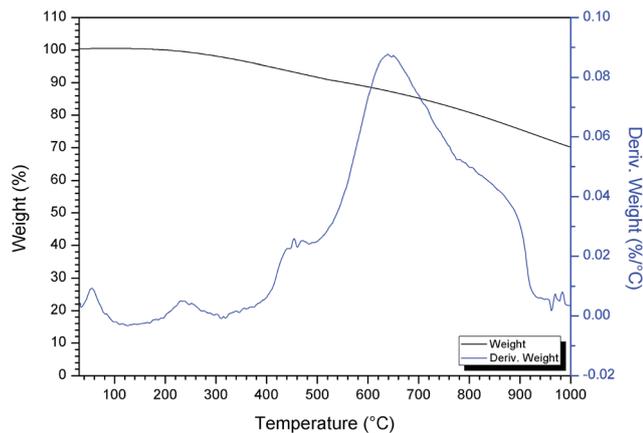
Fig. 3 TG-DTG curves of Ag/AgCl–PANI(10%) photocatalyst.

Fig. 4 UV-visible DRS of the prepared composites.

Fig. 5 PL emission spectra of the Ag/AgCl, Ag/AgCl–PANI(5%), and Ag/AgCl–PANI(20%) photocatalysts.

impurities from the composite.[21] The second weight loss in the range 220–300 °C may be attributed to degradation of aniline oligomers.[22] The third degradation step around 650 °C is due to the decomposition of molecular chains of the polyaniline backbone[21] leading to the formation of small aromatic fragments, substituted aromatic fragments, and extended aromatic fragments.[23,24] The total weight loss between 200 °C and 900 °C can be accounted for only 25% indicating the high thermal stability of the prepared composite.

Specific surface areas of the prepared composites are provided in Table 1. Pure Ag/AgCl has the minimum specific surface area. The introduction of PANI causes a considerable change in the physicochemical characteristics of the resulting photocatalyst composite, as it led to a significant increase in the surface area of the prepared catalysts. Ag/AgCl–PANI(5%) showed the highest surface area and by increasing the content of PANI to more than 5%, the surface area decreased which might be due to the aggregation of PANI over the surface of Ag/AgCl as observed from SEM images. Generally, the high surface area of Ag/AgCl–PANI composite can enhance the adsorption of MB and consequently improve the photocatalytic activity.[7,25]

The UV-visible light DRS were measured to investigate the optical properties of the prepared composites. As illustrated in Fig. 4, pure AgCl shows absorbance only in the UV light region with almost no absorption in the range of 400–800 nm (visible light region).[26] The partial photo-reduction of Ag^{+} in AgCl to prepare Ag/AgCl and Ag/AgCl–PANI composites resulted in high absorption ability in the visible light region (at about 500–650 nm) due to the surface plasmonic resonance of the photo-excited Ag[0] nanoparticles.[27] In case of pure PANI, it absorbs significantly in the UV and visible regions because of the $\pi \rightarrow \pi^*$ transition in the PANI molecules.[15] For Ag/AgCl–PANI
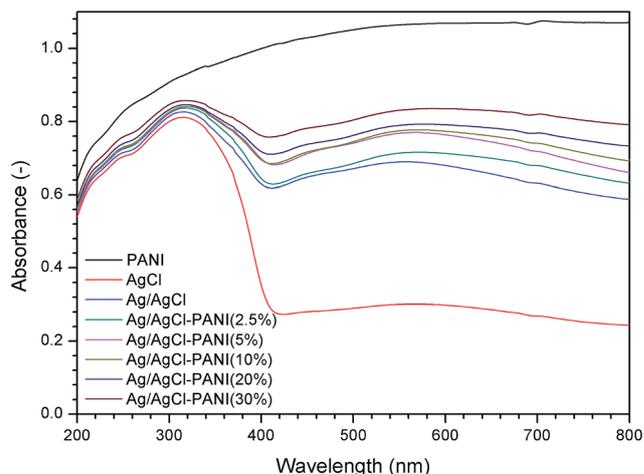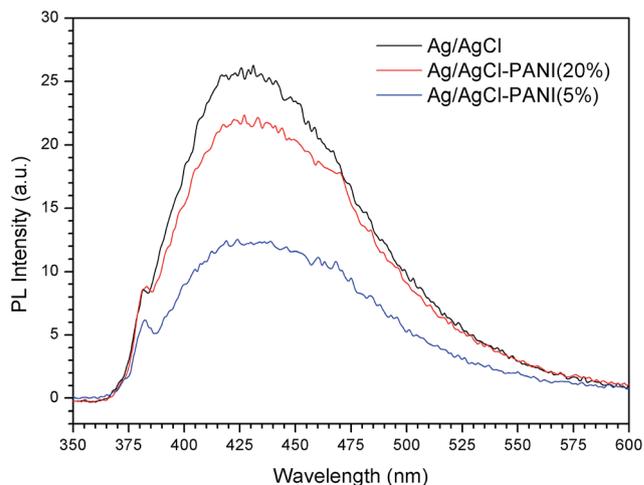
composites, the absorption intensity in the visible light region increases gradually with more PANI content. The same behavior was observed in the previous studies concerned with mixing of PANI with TiO_2 and g-C_3N_4.[16,17] Therefore, Ag/AgCl–PANI composites can be excited efficiently by the solar light to generate more electron–hole pairs than Ag/AgCl.

Photoluminescence spectroscopy was used to evaluate the recombination rate of the photo-generated electrons and holes in the photocatalysts. Fig. 5 presents the PL spectra of pure Ag/AgCl, Ag/AgCl–PANI(5%), and Ag/AgCl–PANI(20%) with an excitation wavelength of 325 nm. Pure Ag/AgCl shows luminous

Table 1 BET surface areas of the prepared composites

| Sample | Ag/AgCl | Ag/AgCl–PANI(x%) | | | |
		x = 2.5%	x = 5%	x = 10%	x = 20%
BET surface area (m^2 g^{-1})	15.18	36.76	53.08	38.50	23.04

peak emerged at 360 to 600 nm with the highest intensity revealing that it possesses the lowest electron–hole pair separation efficiency and low photocatalytic efficiency.[15,16] On contrary, the intensity of Ag/AgCl–PANI(5%) PL emission peak is the lowest one which confirms that PANI aids in the separation of the electron–hole pair and increases the photocatalytic activity. Based on the above analysis, the significant enhancement in photocatalytic activity of Ag/AgCl–PANI can be attributed to the remarkable synergistic effect of hetero-junction structure which formed in the interface between Ag/AgCl and PANI. The emission spectra intensity increase again with Ag/AgCl/PANI(20%) which indicates that the separation efficiency of charge carries decrease again with increasing the content of PANI to 20%. Therefore, the content of PANI plays an important role in the electron–hole pair separation efficiency and in improving the photocatalytic activity of the composite. Regardless the slightly higher recombination rate at high PANI content, it is worth mentioning that Ag/AgCl/PANI(20%) of low efficiency (relative to Ag/AgCl/PANI(5%)) is still more efficient than pure Ag/AgCl photocatalyst.

The pH_{pzc} of Ag/AgCl/PANI(5%) was found to be 5.8 as shown in Fig. 6. At higher pH than pH_{pzc}, catalyst surface is negatively charged and attracts cations, while at pH below pH_{pzc}, catalyst surface is positively charged and repels cations.[19,28]

3.2. Photocatalytic performance

Photocatalytic performance of the prepared photocatalyst composites were assessed based on their ability for the degradation of MB as a function of solar irradiation time. Fig. 7 shows the change of the absorbance at $\lambda_{max} = 664$ nm during photocatalytic degradation of MB using the prepared photocatalyst composites at different conditions. The following rate equation was used to describe the degradation of MB:

$$-\frac{d[MB]}{dt} = k_{app}[MB] \tag{1}$$

where k_{app} is the apparent rate constant for the degradation of MB, [MB] is the concentration of MB, and t (min) is the
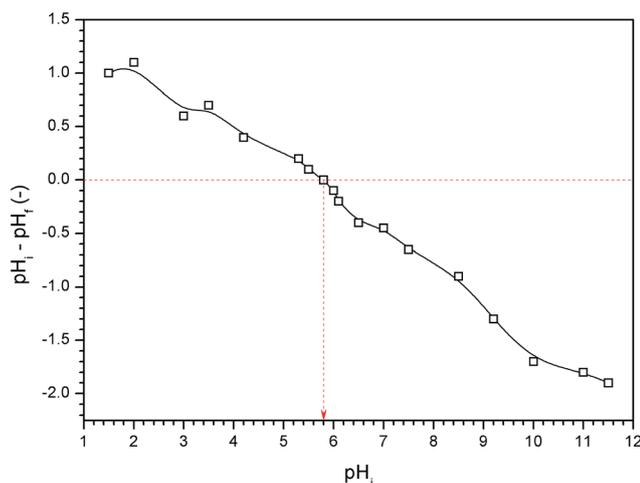

Fig. 6 Point of zero charge of Ag/AgCl–PANI(5%).

irradiation time. The relationship between $\ln([MB]/[MB]_0)$ and the irradiation time of MB degradation resulted in a straight line with R^2 close to unity, which suggests that the degradation behavior obeys the first-order kinetics. Table 2 shows the values of the first-order degradation rate constants k_{app} (min^{-1}) for MB with different experiment conditions. Fig. 7 shows that the experimental point data are fitted with the line of the first order kinetics.

Fig. 7(a), reveals that the degradation rate constant of direct photolysis of the MB in the absence of the photocatalyst is very low ($k_{app} = 1.57 \times 10^{-3}$ min^{-1}) indicating that MB is stable under simulated solar light and the degradation of the dye is only induced when using a photocatalyst. Pure PANI showed poor photocatalytic ability which may be attributed to the unavailability of photo-generated electrons and holes for photocatalytic reaction due to their high recombination rate.[29] Ag/AgCl exhibited low photoactivity with degradation constant of (28×10^{-3} min^{-1}), due to its low surface area too. Besides, mechanical mixture of Ag/AgCl–PANI(5%) has a value of degradation rate constant close to that for pure Ag/AgCl photocatalyst. This is due to the lack of synergistic effect of hetero-junction structure which formed in the interface between Ag/AgCl and PANI. On the other hand, a significant increase in the rate of MB degradation was observed by Ag/AgCl–PANI composites.

It is clear that Ag/AgCl–PANI(5%), exhibits the highest photo-degradation rate constant among the above prepared composite samples, giving a 4.3 times higher than the degradation rate constant of pure Ag/AgCl. The results showed that 5% content of PANI is the best to improve the photocatalytic ability of the Ag/AgCl. Larger contents led to reduced photocatalytic activity as shown in Table 2.

The high surface area of Ag/AgCl–PANI(5%) (53.08 m^2 g^{-1}) led to higher adsorption affinity and photocatalytic activity compared to pure Ag/AgCl and other prepared photocatalyst (see Table 1 and Fig. 7(a)). It was indicated that the surface area is considered as one of the main factor controlling the photocatalytic performance as it would help in concentration, efficient diffusion, and transportation of adsorbed MB dye molecules for the photoreactions which will enhance the photodegradation rate.[30] Moreover, the high surface area can submit high number of active adsorption sites and photocatalytic reaction centers, which would enhance the photo-degradation activity.[7] When the content of PANI increased over 5%, it was aggregated over the surface of Ag/AgCl as shown in SEM images (Fig. 2) leading to lower surface area. Therefore the adsorption ability of the photocatalysts reduced, and finally the degradation rate of the photocatalytic reaction decreased.[31]

From the SEM, and UV-vis absorption spectra results, it was clear that PANI is spreaded over the surface of Ag/AgCl and an enhanced absorption intensity of the composite in visible region was observed. While at high content of PANI (Ag/AgCl–PANI(20%)), PANI aggregated on the surface of photocatalyst and reduced the light hitting the surface of Ag/AgCl particles.

In addition, Ag/AgCl–PANI(5%) exhibited the lowest emission intensity indicating that this composite possesses the highest separation efficiency of the photo-generated electrons
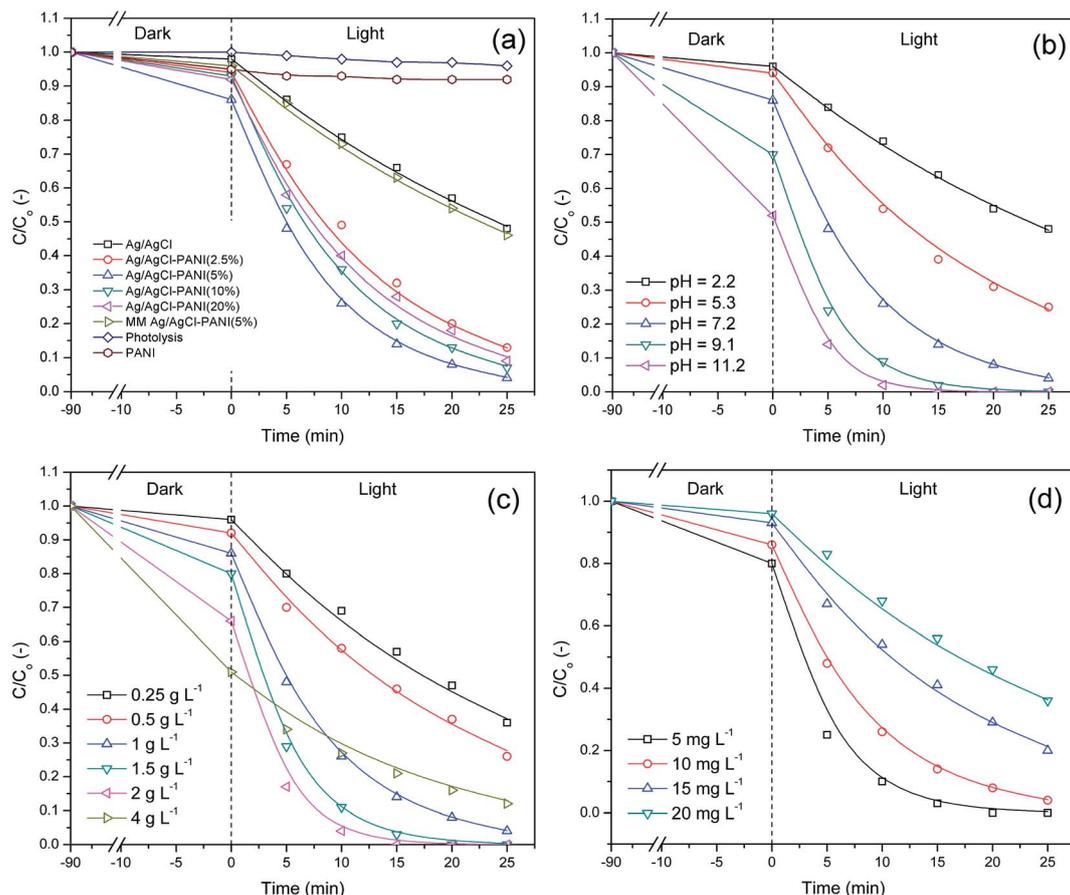
Fig. 7 Photo-degradation of MB by Ag/AgCl–PANI nanocomposites under simulated solar light irradiation; (a) effect of PANI content (photo-catalyst dose = 1 g L^{-1}, MB initial concentration ([MB]$_0$) = 10 mg L^{-1}, pH 7.2), (b) effect of pH (photocatalyst dose = 1 g L^{-1}, [MB]$_0$ = 10 mg L^{-1}), (c) effect of photocatalyst dose ([MB]$_0$ = 10 mg L^{-1}, pH 7.2), and (d) effect of MB initial concentration (photocatalyst dose = 1 g L^{-1}, pH 7.2). Points represent the experimental values and lines represent the 1st order kinetics.

and holes. The increase in PANI ratio more than 5% lead to increases in PL emission intensity, which is a result of low electron–hole separation efficiency (see Fig. 5), and may be also a good interpretation for the decreasing the photocatalytic activity of the composite with high PANI ratio. These results indicate that the content of PANI plays an important role in improving the photoactivity of Ag/AgCl.

The pH is an important factor that affects the activity of the composite as it may change the photocatalyst surface properties and the ionic nature of the treated compound. Thus, the influence of pH on the degradation of MB using the best most performance photocatalyst Ag/AgCl–PANI(5%) is presented in Fig. 7b.

The adsorption of pollutant molecule onto catalyst surface is highly influenced by pH at point of zero charge (pH$_{pzc}$) of the prepared catalyst.[19] pH$_{pzc}$ explains the increase in the adsorption of MB (cationic dye) by Ag/AgCl–PANI(5%) in a medium of pH higher than 5.8 and the decrease in acidic medium (at pH lower than 5.8). The highest degradation rate for MB is observed at pH 11.2 due to high adsorption of the cationic dye molecules. The adsorption capability of the composite increases sharply with increasing the pH value from acidic to alkaline and consequently enhances the photocatalytic degradation rate of

MB. In addition, more hydroxide ions (HO$^-$) are available at higher pH facilitating the formation of HO$^{\bullet}$ in high concentration after reaction with the holes in photocatalyst.[28]

In order to assess the effect of photocatalyst loading on MB dye degradation rate, we performed the experiment using 0.25–4 g L^{-1} Ag/AgCl–PANI(5%) photocatalyst in 70 mL of 10 mg L^{-1} MB at pH 7.2. The MB removal efficiencies were found to increase gradually with increasing the catalyst loading reaching maximum degradation efficiency at 2 g L^{-1} (see Table 2). Further increase in the catalyst loading to 4 g L^{-1} led to a decrease in MB degradation rate under the same experimental conditions. The increase in the catalyst loading leads to an increase in the number of active sites on the photocatalyst surface, which in turn increases the formation rate of active species.[28] However, when the catalyst loading exceeded the limiting value, the MB degradation rate would decrease due to two reasons. The first reason is the increase in turbidity and light scattering at high photocatalyst concentrations which lead to a decrease in the light path inside the solution.[32] The second one is that at high concentrations, Ag/AgCl–PANI(5%) composite can aggregate causing a decrease in the number of photocatalytic active sites.[25]

Table 2 The apparent first-order rate constants in terms of irradiation time obtained for the degradation experiments of different composites

Experiment	k_{app} (min^{-1}) $\times 10^{-3}$	R^2
Photolysis	1.57	0.953
PANI	1.63	0.952
Ag/AgCl	28	0.997
Ag/AgCl–PANI(2.5%)	80	0.994
Ag/AgCl–PANI(5%)	121	0.999
Ag/AgCl–PANI(10%)	101	0.997
Ag/AgCl–PANI(20%)	88	0.986
Mixture of Ag/AgCl : PANI (95 : 5)	29	0.995
pH value		
(—)	k_{app} (min^{-1}) $\times 10^{-3}$	R^2
2.2	28	0.997
5.3	54	0.995
7.2	121	0.999
9.1	232	0.999
11.2	325	0.987
Photocatalyst dose (g L^{-1})	k_{app} (min^{-1}) $\times 10^{-3}$	R^2
0.25	38	0.991
0.5	48	0.991
1	121	0.999
1.5	216	0.995
2	280	0.999
4	55	0.993
MB initial concentration (mg L^{-1})	k_{app} (min^{-1}) $\times 10^{-3}$	R^2
5	215	0.997
10	121	0.999
15	59	0.993
20	39	0.995

Fig. 8 Photo-degradation rate constants of MB using Ag/AgCl–PANI(5%) in presence of different scavengers.

respectively.[7,9,24] MB degradation using Ag/AgCl–PANI(5%) in presence of scavengers is shown in Fig. 8. Under simulated solar light, the degradation rate of MB decreases slightly from 0.121 to 0.110 min^{-1} after adding 10 mM of IPA (70 μL of 10 M IPA in 70 mL MB solution). By increasing the concentration of IPA to 100 mM (700 μL of 10 M IPA in 70 mL MB solution), the degradation were slightly affected, as the degradation reduced to be 0.098 min^{-1} which indicates that HO$^{\bullet}$ has a minor role in the photocatalytic process. On contrary, the degradation rate of MB decreased sharply from 0.121 to 0.004 and 0.001 min^{-1} after adding 1 mM (7 μL of 10 M AO in 70 mL MB solution) and 10 mM (70 μL of 10 M AO in 70 mL MB solution) of AO, respectively. Similarly, the addition of 1 mM (7 μL of 10 M BQ in 70 mL MB solution) and 10 mM (70 μL of 10 M BQ in 70 mL MB solution) of BQ reduced the degradation rate from 0.121 to 0.005 and 0.003 min^{-1}, respectively. Thus, the contribution of oxidizing species in the MB photo-degradation process follows the order: h$^+$ > O$_2^{\bullet-}$ > HO$^{\bullet}$. These results support that h$^+$ and O$_2^{\bullet-}$ are the main active species in the photocatalytic process.

A mechanism describing the photocatalytic degradation of MB using Ag/AgCl–PANI composite under simulated solar light irradiation was suggested based on the results of photocatalytic degradation and photo-generated carriers scavenger experiments (Fig. 9). The conduction band and valence band potentials of AgCl are −0.09 and +3.16 eV (vs. NHE).[9,34] While, the highest occupied molecular orbital (HOMO) and the lowest unoccupied molecular orbital (LUMO) of PANI which are +0.8 eV and −1.9 eV (vs. NHE), respectively.[15,35] This means that the energy band of both AgCl and PANI matches well, which facilitates the transfer of photo-generated electrons in the LUMO of PANI to the conduction band (CB) of the AgCl. At the same time, holes on the VB of AgCl migrate to the HOMO of PANI.

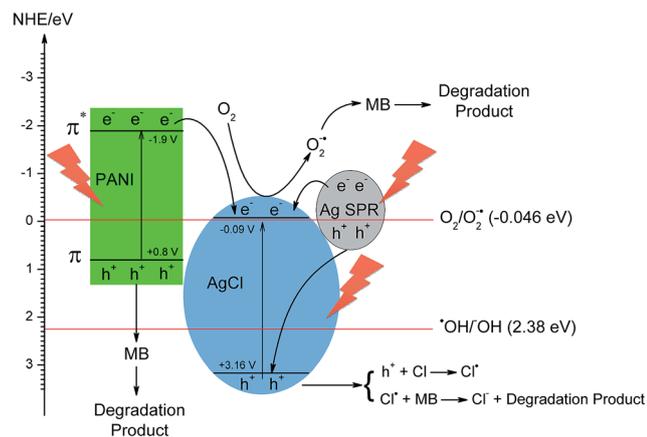Under simulated solar light irradiation, PANI absorbs photons to induce π–π* (HOMO–LUMO) transition,[14,16,17]

Initial concentration of MB dye is another important factor that deserves to be studied. It was examined using various dye concentrations from 5 to 20 mg L^{-1} with a constant Ag/AgCl–PANI(5%) catalyst loading of 70 mg at pH 7.2 (see Fig. 7d). The photo-degradation efficiency increased with decreasing the dye concentration. The adsorption of MB dye by photocatalyst increases as its concentration decrease, and subsequently the photo-degradation rate increases (see Table 2). Furthermore, light passes through the dye solution is partly absorbed by the high concentration of dye which in turn reduced the absorption of photons by the active sites of catalyst. Consequently, the number of photo-generated active radicals formed on the catalyst surface would decrease.[33]

In order to investigate the mechanism of the photocatalytic reaction, the role of the photo-induced reactive species including HO$^{\bullet}$, h$^+$ and O$_2^{\bullet-}$ were evaluated. Trapping experiments were carried out using a series of active scavengers that were added during the photocatalytic process. In this study, IPA, AO and BQ were introduced as scavengers for HO$^{\bullet}$, h$^+$, and O$_2^{\bullet-}$,

Fig. 9 Suggested photocatalytic mechanism for MB degradation using Ag/AgCl–PANI(5%) composite under solar light irradiation.
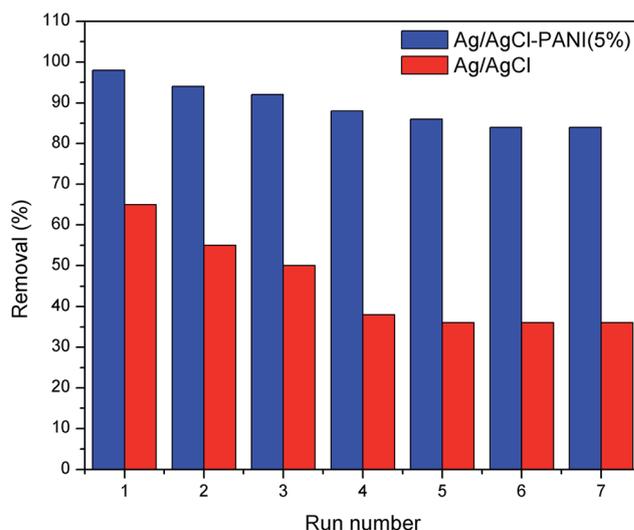

Fig. 10 Reusability of pure Ag/AgCl and Ag/AgCl–PANI(5%) photocatalysts for MB degradation after 25 min irradiation at the same experimental conditions.
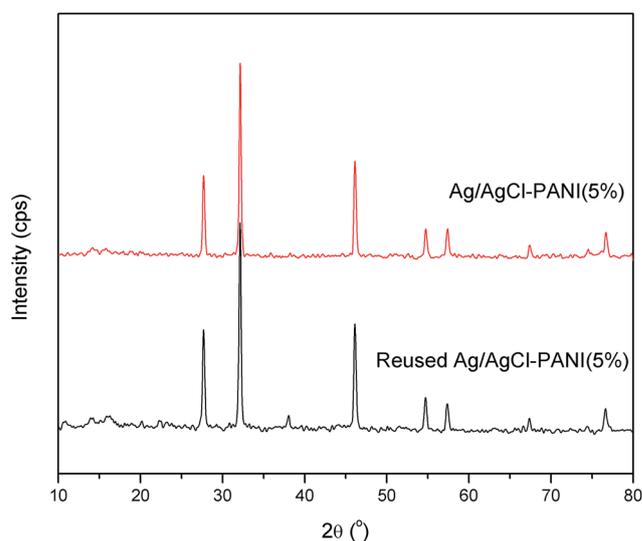

Fig. 11 XRD patterns of the photocatalyst before and after seven successive runs.

transporting the excited-state electrons to the π^*-orbital (LUMO) which is more negative than the CB of AgCl. The excited-state electrons in PANI can transfer to CB of AgCl. At the same time, a large amount of electron–hole (e^-–h^+) pairs are generated due to SPR effect of Ag NPs and the photo-generated electrons transfers to the conduction band of AgCl.[7,9,36] The photo-generated electrons at CB of AgCl with the transferred electrons from PANI and Ag NPs can easily react with O_2 to produce superoxide ion $O_2^{\bullet-}$, as the CB potential of AgCl (-0.09 eV $vs.$ NHE) is more negative than that of $O_2/O_2^{\bullet-}$ (-0.046 eV $vs.$ NHE).[9,34] Furthermore, as PANI is a good material for transporting holes[14–16,24,37] the photo-generated holes left in both PANI and Ag can transfer to the surface of the photocatalyst and react directly with adsorbed MB molecules and oxidize organic pollutants rather than produce HO$^{\bullet}$ because the potentials of HO$^{\bullet}$/HO$^-$ (2.38 eV $vs.$ NHE)[38,39] are more positive than both the HOMO energy level of PANI and the Fermi level of Ag NPs.[40,41] In addition, the photo-generated holes in VB of AgCl including the transferred holes from Ag NPs can transfer to the AgCl surface and oxidize Cl^- to $Cl^{\bullet}$. These $Cl^{\bullet}$ are reactive radical species that can oxidize MB and then regenerate Cl^- ions for the next catalytic cycle. They can also directly react with the adsorbed MB on catalyst surface, and only a few of them can react with the adsorbed water (or hydroxide anions) to produce HO$^{\bullet}$ radicals.[7,37] Because of the synergy between Ag, AgCl and PANI, the recombination rate between photo-generated electron and holes reduced which improve the photocatalytic activity of the photocatalyst.

Stability of the photocatalyst is an important issue for the practical application. The stability of pure Ag/AgCl and Ag/AgCl–PANI(5%) composite was investigated through seven consecutive experiments at the same conditions. As shown in Fig. 10, the degradation of MB over pure Ag/AgCl decreased from 65% (in the first experiment) to 36% after seven cycles, respectively. This result is consistent with the findings of previous studies.[5,26] The degradation over Ag/AgCl–PANI(5%) decreased also but with much less extent (from 98% to 84% after seven cycles, respectively) indicating that PANI not only improves the photo-

degradation performance of Ag/AgCl, but also enhances its stability.

The used Ag/AgCl–PANI(5%) sample was collected after seven cycles and was checked using XRD analysis (see Fig. 11) to monitor the changes in its crystallographic structure. It was revealed that used photocatalyst possesses comparable XRD pattern to that of the as-prepared fresh sample, except for the peaks characteristic for metallic Ag, which can be indexed to the cubic phase of Ag (JCPDS file: 65-2871). This result validates that Ag/AgCl–PANI(5%) composite is a kind of active and stable photocatalyst and can be used for long-term practical application.

4. Conclusions

In summary, a novel plasmonic photocatalysts, Ag/AgCl–PANI, were successfully synthesized by *in situ* formation followed by photo-reduction of Ag^+ into Ag^0 on the surface of AgCl which distributed on the surface of PANI. The prepared photocatalysts exhibit high efficiency for the degradation of MB under simulated solar light irradiation as compared to pure PANI and Ag/AgCl. The photocatalytic activity and stability of Ag/AgCl is improved after introducing PANI into the prepared photocatalyst. PANI improves the surface area and increases the visible-light absorption ability of the prepared photocatalysts. Furthermore the enhanced photocatalytic activity and stability of the photocatalysts can be attributed to the presence of synergistic effect of hetero-junction structure formed in the interface between Ag/AgCl and PANI which is effective in separation of photoexcited electron–hole pairs. Ag/AgCl–PANI(5%) showed the highest photocatalytic performance with a rate constant ~4 times higher than that of the pure Ag/AgCl. However, increasing the percentage of PANI to more than 5% led to a reduction in electron–hole separation efficiency, decreasing the surface area of the photocatalyst, and can cover the surface of Ag/AgCl and hinders the light absorption intensity of AgCl, thus decreasing its photocatalytic activity. The trapping of oxidizing species during MB photo-degradation helped in the estimation of a possible mechanism for the photo-degradation of MB molecules under simulated solar irradiation. It was found that the hydroxyl radicals ($HO^•$) have negligible oxidation effect compared with holes (h^+) and superoxide radicals $O_2^{•−}$.

Acknowledgements

References

1 X. Lang, X. Chen and J. Zhao, Heterogeneous visible light photocatalysis for selective organic transformations, *Chem. Soc. Rev.*, 2014, **43**(1), 473–486.

2 D. Xiao, *et al.*, Sheet-like and truncated-dodecahedron-like AgI structures *via* a surfactant-assisted protocol and their morphology-dependent photocatalytic performance, *Phys. Chem. Chem. Phys.*, 2017, **19**(1), 837–845.

3 S. Zhang, *et al.*, Rationally designed 1D Ag@AgVO$_3$ nanowire/graphene/protonated g-C$_3$N$_4$ nanosheet heterojunctions for enhanced photocatalysis *via* electrostatic self-assembly and photochemical reduction methods, *J. Mater. Chem. A*, 2015, **3**(18), 10119–10126.

4 X. Zhou, *et al.*, Surface plasmon resonance-mediated photocatalysis by noble metal-based composites under visible light, *J. Mater. Chem.*, 2012, **22**(40), 21337–21354.

5 H. Daupor and S. Wongnawa, Urchinlike Ag/AgCl photocatalyst: Synthesis, characterization, and activity, *Appl. Catal., A*, 2014, **473**, 59–69.

6 M. Zhu, P. Chen and M. Liu, Ag/AgBr/graphene oxide nanocomposite synthesized *via* oil/water and water/oil microemulsions: a comparison of sunlight energized plasmonic photocatalytic activity, *Langmuir*, 2012, **28**(7), 3385–3390.

7 X. Xu, *et al.*, SiO$_2$@Ag/AgCl: a low-cost and highly efficient plasmonic photocatalyst for degrading rhodamine B under visible light irradiation, *RSC Adv.*, 2014, **4**(110), 64747–64755.

8 H. Zhang, *et al.*, Graphene sheets grafted Ag@AgCl hybrid with enhanced plasmonic photocatalytic activity under visible light, *Environ. Sci. Technol.*, 2011, **45**(13), 5731–5736.

9 S. Zhang, *et al.*, In situ ion exchange synthesis of strongly coupled Ag@AgCl/g-C$_3$N$_4$ porous nanosheets as plasmonic photocatalyst for highly efficient visible-light photocatalysis, *ACS Appl. Mater. Interfaces*, 2014, **6**(24), 22116–22125.

10 M. Zhu, P. Chen and M. Liu, Graphene oxide enwrapped Ag/AgX (X = Br, Cl) nanocomposite as a highly efficient visible-light plasmonic photocatalyst, *ACS Nano*, 2011, **5**(6), 4529–4536.

11 M. Zhu, P. Chen and M. Liu, Highly efficient visible-light-driven plasmonic photocatalysts based on graphene oxide-hybridized one-dimensional Ag/AgCl heteroarchitectures, *J. Mater. Chem.*, 2012, **22**(40), 21487–21494.

12 M. Zhu, P. Chen and M. Liu, High-performance visible-light-driven plasmonic photocatalysts Ag/AgCl with controlled size and shape using graphene oxide as capping agent and catalyst promoter, *Langmuir*, 2013, **29**(29), 9259–9268.

13 K. Lee, *et al.*, Metallic transport in polyaniline, *Nature*, 2006, **441**(7089), 65–68.

14 Y. Bu and Z. Chen, Role of Polyaniline on the Photocatalytic Degradation and Stability Performance of the Polyaniline/Silver/Silver Phosphate Composite under Visible Light, *ACS Appl. Mater. Interfaces*, 2014, **6**(20), 17589–17598.

15 Q. Wang, *et al.*, Photodegradation of methyl orange with PANI-modified BiOCl photocatalyst under visible light irradiation, *Appl. Surf. Sci.*, 2013, **283**, 577–583.

16 L. Ge, C. Han and J. Liu, In situ synthesis and enhanced visible light photocatalytic activities of novel PANI–gC$_3$N$_4$ composite photocatalysts, *J. Mater. Chem.*, 2012, **22**(23), 11843–11850.

17 H. Zhang, *et al.*, Dramatic visible photocatalytic degradation performances due to synergetic effect of TiO$_2$ with PANI, *Environ. Sci. Technol.*, 2008, **42**(10), 3803–3807.

18 S. Fathalipour and B. Massoumi, Preparation of AgCl/polyanilalcohol nanocomposite in polyvinylalcohol matrix and its electrocatalytic activity, *J. Appl. Polym. Sci.*, 2015, **132**(35), 42366.

19 O. Bechambi, S. Sayadi and W. Najjar, Photocatalytic degradation of bisphenol A in the presence of C-doped ZnO: effect of operational parameters and photodegradation mechanism, *J. Ind. Eng. Chem.*, 2015, **32**, 201–210.

20 S. Zhang, *ACS Appl. Mater. Interfaces*, 2014, **6**(24), 22116–22125.

21 W. Wang, *et al.*, Ferrite-grafted polyaniline nanofibers as electromagnetic shielding materials, *J. Mater. Chem. C*, 2013, **1**(16), 2851–2859.

22 A. Elsayed, *et al.*, Synthesis and properties of polyaniline/ferrites nanocomposites, *Int. J. Electrochem. Sci.*, 2011, **6**, 206–221.

23 M. O. Ansari and F. Mohammad, Thermal stability and electrical properties of dodecyl-benzene-sulfonic-acid doped nanocomposites of polyaniline and multi-walled carbon nanotubes, *Composites, Part B*, 2012, **43**(8), 3541–3548.

24 Y. Lin, *et al.*, Highly efficient photocatalytic degradation of organic pollutants by PANI-modified TiO_2 composite, *J. Phys. Chem. C*, 2012, **116**(9), 5764–5772.

25 A. Pourahmad, S. Sohrabnezhad and E. Kashefian, AgBr/nano AlMCM-41 visible light photocatalyst for degradation of methylene blue dye, *Spectrochim. Acta, Part A*, 2010, **77**(5), 1108–1114.

26 B. Ma, *et al.*, Highly stable and efficient Ag/AgCl core–shell sphere: controllable synthesis, characterization, and photocatalytic application, *Appl. Catal., B*, 2013, **130**, 257–263.

27 Z. Lou, *et al.*, Synthesis and activity of plasmonic photocatalysts, *ChemCatChem*, 2014, **6**(9), 2456–2476.

28 M. Barakat, *et al.*, Photocatalytic degradation of 2-chlorophenol by Co-doped TiO_2 nanoparticles, *Appl. Catal., B*, 2005, **57**(1), 23–30.

29 H. Zhang, *et al.*, One-step modified method for a highly efficient Au–PANI@TiO_2 visible-light photocatalyst, *New J. Chem.*, 2016, **40**(10), 8587–8592.

30 J. Hou, *et al.*, Hierarchically plasmonic Z-scheme photocatalyst of Ag/AgCl nanocrystals decorated mesoporous single-crystalline metastable $Bi_{20}TiO_{32}$ nanosheets, *J. Phys. Chem. C*, 2013, **117**(10), 5132–5141.

31 Y. Chen, *et al.*, Construction of heterostructured g-C_3N_4/Ag/TiO_2 microspheres with enhanced photocatalysis performance under visible-light irradiation, *ACS Appl. Mater. Interfaces*, 2014, **6**(16), 14405–14414.

32 S. Sakthivel, *et al.*, Solar photocatalytic degradation of azo dye: comparison of photocatalytic efficiency of ZnO and TiO_2, *Sol. Energy Mater. Sol. Cells*, 2003, **77**(1), 65–82.

33 C.-C. Wang, *et al.*, Photocatalytic degradation of CI Basic Violet 10 using TiO_2 catalysts supported by Y zeolite: an investigation of the effects of operational parameters, *Dyes Pigm.*, 2008, **76**(3), 817–824.

34 L. Ye, *et al.*, Two different roles of metallic Ag on Ag/AgX/BiOX (X = Cl, Br) visible light photocatalysts: surface plasmon resonance and Z-scheme bridge, *ACS Catal.*, 2012, **2**(8), 1677–1683.

35 G. Senadeera, *et al.*, Deposition of polyaniline *via* molecular self-assembly on TiO_2 and its uses as a sensitiser in solid-state solar cells, *J. Photochem. Photobiol., A*, 2004, **164**(1), 61–66.

36 C. An, S. Peng and Y. Sun, Facile Synthesis of Sunlight-Driven AgCl: Ag Plasmonic Nanophotocatalyst, *Adv. Mater.*, 2010, **22**(23), 2570–2574.

37 P. Xiong, *et al.*, Ternary titania–cobalt ferrite–polyaniline nanocomposite: a magnetically recyclable hybrid for adsorption and photodegradation of dyes under visible light, *Ind. Eng. Chem. Res.*, 2013, **52**(30), 10105–10113.

38 H. Cheng, *et al.*, One-step synthesis of the nanostructured AgI/BiOI composites with highly enhanced visible-light photocatalytic performances, *Langmuir*, 2010, **26**(9), 6618–6624.

39 H. Ji, *et al.*, Magnetic gC_3N_4/$NiFe_2O_4$ hybrids with enhanced photocatalytic activity, *RSC Adv.*, 2015, **5**(71), 57960–57967.

40 M. Xu, L. Han and S. Dong, Facile fabrication of highly efficient g-C_3N_4/Ag_2O heterostructured photocatalysts with enhanced visible-light photocatalytic activity, *ACS Appl. Mater. Interfaces*, 2013, **5**(23), 12533–12540.

41 X. Yao, X. Liu and X. Hu, Synthesis of the Ag/AgCl/g-C_3N_4 Composite with High Photocatalytic Activity under Visible Light Irradiation, *ChemCatChem*, 2014, **6**(12), 3409–3418.